Retina

Imaging Retinal Capillaries Using Ultrahigh-Resolution Optical Coherence Tomography and Adaptive Optics

Qiang Wang,[1] *Omer P. Kocaoglu,*[1] *Barry Cense,*[1,2] *Jeremy Bruestle,*[1] *Ravi S. Jonnal,*[1] *Weihua Gao,*[1] *and Donald T. Miller*[1]

Purpose. Ultrahigh-resolution optical coherence tomography (UHR-OCT) with adaptive optics (AO) provides micrometer-scale 3D resolution that is attractive for imaging the retinal microvasculature. Such imaging may be useful for early detection of pathologic changes as in diabetic retinopathy. Here the authors investigate this potential for detecting individual capillaries in healthy subjects.

Methods. UHR-AO-OCT volumes centered on the fovea were acquired from seven subjects (age range, 25–61 years) with three preselected with no foveal avascular zone (FAZ). Images were compared with entoptic diagrams using the capillaries at the rim of the FAZ. Methods of comparison were testing for the presence of a FAZ, noting distinct features in the capillary pattern, and measuring the size of the FAZ. Additional analysis included measurements of capillary diameter and depth range with retinal eccentricity.

Results. UHR-AO-OCT results are consistent with entoptic observations for all three methods of comparison. FAZ diameters measured by UHR-AO-OCT and entoptic imaging are strongly correlated ($R^2 = 0.86$). Average capillary diameter near the FAZ rim is 5.1 (4.6) $\pm$ 1.4 μm, with the value in parentheses accounting for axial image blur. This is consistent with histology (average, ~4.7 μm). Depth range of the capillaries increases monotonically with eccentricity (0°–1.25°) and is larger and more variable for subjects without FAZ.

Conclusions. UHR-AO-OCT permits observation of many of the capillaries proximal to the FAZ, including those of average size based on published histology. This supports the view that the vast majority of capillaries in the retina are likely detectable with UHR-AO-OCT. (*Invest Ophthalmol Vis Sci.* 2011;52:6292–6299) DOI:10.1167/iovs.10-6424

The retinal vasculature is a complex, layered network of vessels and capillary beds that permeate the retina. They provide a steady supply of nutrients and dispose of cellular byproducts, both essential for maintaining retinal health and function. Compromise of this support system has severe consequences to the retina and often underlies retinal abnormalities, in particular diabetic retinopathy, a leading cause of blindness in the Western world. Fluorescein angiography (FA)[1–7] and entoptic viewing[8–15] are established methods for observing fine details of the retinal vasculature and early pathologic changes. Both techniques, however, are not without shortcomings. FA requires injection of a toxic fluorescent dye and fails to detect a significant fraction of capillaries, especially those with small diameters, because of its poor depth sectioning capability and sensitivity to quality of the angiogram (optical quality of the eye). In spite of these shortcomings, FA has been used to measure the retinal microcirculation (e.g., capillary blood flow velocity[5–7]), area between capillaries,[6] and FAZ size.[1–4,6]

Entoptic viewing is a psychophysical method that allows self-visualization of the retinal vasculature or, more specifically, the shadow patterns the vasculature casts during illumination of the retina. Unlike FA, entoptic viewing is noninvasive, unaffected by the eye's optics, and limited to the fovea for viewing capillaries. In this localized area, the method has been used to study foveal capillary details, FAZ size and shape,[8–10] foveal vessels,[9–11] macular blood flow,[12,13] and capillary density around the FAZ.[14] It has also been compared with fluorescein angiography and shown to contain more foveal capillary detail.[15]

More recently, retinal imaging instruments equipped with adaptive optics (AO) have garnered considerable interest for imaging the retinal microvasculature. AO increases imaging resolution and sensitivity, both advantageous for detecting small, weakly reflecting capillaries. AO scanning laser ophthalmoscopes (AO-SLOs) have been used to map the local 2D distribution and flow dynamics of the retinal microvasculature in living eyes.[16–18] AO retina cameras based on flood illumination have also demonstrated similar imaging capability.[19] AO has been incorporated into optical coherence tomography (OCT).[20–27] The major advantage of OCT is its substantially higher axial resolution[28,29] (~3–8 μm compared with >60 μm for AO-SLO and AO flood-illumination retina cameras), which, when combined with AO, offers the potential to map the microvasculature in all three dimensions to differentiate, for example, the multilaminar networks of capillaries.

There have been reports of AO-OCT imaging of retinal capillaries,[23–25,30–32] in particular that by Hammer et al.,[24] who compared the diameters of capillaries of patients with retinopathy of prematurity with those of persons without it. The vasculature detail realized with these instruments is impressive, yet the qualitative nature of these observations along with the quantitative analysis of Hammer et al.[24] do not address whether the capillaries are faithfully imaged. This raises a fundamental issue about the capacity of AO-OCT to image capillaries, whose size varies considerably (2.5–7 μm[33]; 2.5–10 μm[34]) and that network with vessels of increasingly larger size. Certainly the AO-SLO mapping of the small capillaries near the rim of the FAZ suggests AO-OCT is capable of the same, but this has yet to be demonstrated. Moreover, AO-SLO and AO-OCT instruments are fundamentally different. The interferometric nature of AO-OCT results in high-contrast speckle that permeates

the AO-OCT image and confounds the detection of structures that approach the size of speckle (e.g., comparable to the diameters of small capillaries). The much slower image acquisition of AO-OCT compared with AO-SLO (100–1000 times slower) also leads to larger and more disruptive motion artifacts that degrade the image and obstruct visualization of capillaries.

Given these unknowns, we investigated the capability of an ultrahigh-resolution AO OCT system (UHR-AO-OCT) to image capillaries in a 3° × 3° region centered on the fovea. This region[35–37] is occupied by the FAZ and the network of capillaries that define its terminal rim. Use of the rim capillaries enabled us to compare the UHR-AO-OCT images with entopic viewing, an independent and established psychophysical method for mapping foveal capillaries[8–15] on the same seven subjects. Comparisons were made in terms of presence or absence of a FAZ, gross dimensions of the FAZ, and qualitative characteristics of capillary patterns unique to specific eyes. In addition, UHR-AO-OCT measurements of the capillary diameter and depth variation with retinal eccentricity are reported.

SUBJECTS AND METHODS

Subjects

We recruited seven subjects for UHR-AO-OCT and entoptic measurements. The subjects ranged in age from 25 to 61 years (average ± SD, 37.1 ± 14.5). All were free of ocular disease and had normal corrected vision. Age, presence of FAZ, refractive error, visual acuity, and axial length for each subject are listed in Table 1. To facilitate comparison of the two measurement techniques, 3 of the 7 subjects were preselected with no FAZ, a condition present in only a small portion of the population.[38,39]

Description of the UHR-AO-OCT Instrument

The UHR-AO-OCT system used for this study is described in detail elsewhere.[30] In short, the UHR-AO-OCT is a fiber-based Michelson interferometer that contains an ultra-broadband superluminescent diode and a woofer-tweeter AO system to achieve a 3D resolution of approximately 3 × 3 × 3 μm^3 in retinal tissue. The AO component consists of a Shack-Hartmann wavefront sensor (SHWS) for measuring ocular aberrations, an AOptix (Campbell, CA) deformable mirror (DM) (37 electrodes; 16-μm stroke) for correction of primarily low-order aberrations, and a Boston MicroMachines Corporation (BMC; Cambridge, MA) DM (140 actuators; 3.8-μm stroke) for correction of primarily high-order aberrations. The ocular aberrations are dynamically corrected at 22.5 Hz during UHR-AO-OCT image acquisition. Before acquisition, the AOptix mirror adjusts focus in the thick retina for optimal visibility of the retinal vasculature, the retinal feature of interest for this study. The UHR-OCT light source is a superluminescent diode (BroadLighter; Superlum Diodes Ltd., Moscow, Russia) with 110-nm bandwidth, 840-nm center wavelength, and 12-mW output

power. The OCT control and acquisition software was upgraded to a 64-bit platform and recoded in C# and C++ for increased volume acquisition and storage, faster processing, and enhanced user control. UHR-AO-OCT A-scans were acquired at a rate of 22.5 kHz.

Procedure for UHR-AO-OCT Experiment

Procedures on human subjects strictly adhered to the tenets of the Declaration of Helsinki and the Institutional Review Board of Indiana University. Measurements were performed in the right eyes of the seven volunteers. Before UHR-AO-OCT measurements, 1 drop of 0.5% tropicamide was applied topically to the subject's eye for pupil dilation and paralysis of accommodation. A bite bar mount attached to a three-axis positioning stage stabilized the subject's head. The subject's line of sight was coaligned to the optical axis of the UHR-AO-OCT system, permitting volume images to be acquired of the fovea. This alignment was realized by the subject fixating on a visual target positioned on the optical axis of the UHR-AO-OCT system and lateral alignment of the subject's pupil such that the UHR-AO-OCT beam passed through the pupil center.

For two of the subjects, trial lenses were added to coarsely remove large levels of defocus and astigmatism that could not be adequately removed with the AO system. AO was initiated (AOptix first, then BMC) followed by dynamic correction (BMC only) during the UHR-AO-OCT volume acquisition. Coarse adjustment in focus was guided by image quality of the UHR-AO-OCT image displayed in real time on the computer monitor. Fine adjustment of focus entailed acquiring a series of UHR-AO-OCT volumes of the same patch of retina with slightly different focus (typically ±0.05 D) to ensure clear images of capillaries were acquired. This two-step focus procedure (coarse and fine) minimized the impact of focus error on the clarity of individual capillaries.

Maximum power delivered to the eye was ~400 μW, which complies with the ANSI standard.[40] Care was taken to axially position the retina of each subject so that it resided roughly 500 μm from the zero-delay point of the UHR-AO-OCT. In this way, fluctuations in dynamic range caused by sensitivity drop-off of the spectrometer were minimized. UHR-AO-OCT volumes were acquired of 3° × 3° (~900 × 900 μm) retinal patches. A 3° field was selected to ensure coverage of the retinal capillary network that defines the rim of the FAZ, which is typically 1.5° to 2.5° in diameter.[6,10,39] Each volume consisted of 100 B-scans of 1000 A-scans each (4.4 seconds) nominally centered on the fovea (line of sight). B-scan spacing was purposefully coarser to enable rapid acquisition of large volumes and to reduce the impact of eye motion and tear film artifacts.

Volumes were selected for postprocessing that exhibited minimal motion artifacts and provided best clarity of the retinal vasculature. Typically, this meant selecting the best volume from among several acquired of the same retinal location. Using ImageJ software (developed by Wayne Rasband, National Institutes of Health, Bethesda, MD; available at http://rsb.info.nih.gov/ij/index.html) with the "StackReg" plug-in (developed by Philippe Thévenaz, Biomedical Imaging Group, Swiss Federal Institute of Technology Lausanne; available at http://

TABLE 1. Subject Age, Presence of FAZ, Refractive Error, Best-Corrected Visual Acuity, and Axial Length

Subject	Age (y)	Presence of a FAZ	Refractive Error (D)	Visual Acuity (letter)	Axial Length (mm)
1	25	Yes	−4.25 S −1.00 × 010	20/20	26.40
2	25	Yes	Plano	20/15	23.70
3	30	Yes	−3.0 S	20/10	26.06
4	30	Yes	−4.5 S −0.25 × 055	20/20	24.87
5	35	No	−2.75 S −1.25 × 180	20/20	25.37
6	54	No	+0.75 S −0.25 × 045	20/15	23.49
7	61	No	−0.5 S −0.5 × 090	20/15	24.14

Eye length was measured with an optical biometer (IOLMaster; Carl Zeiss Meditec, Jena, Germany). All ocular parameters are for the subjects' right eye.

bigwww.epfl.ch/thevenaz/stackreg/), 100 preprocessed B-scans were registered. The registration was constrained to the *x-z* (B-scan) plane involving *x* and *z* shift and single-axis rotation; individual A-scans were not adjusted relative to each other. The volumes were then cropped to eliminate the empty space generated by the registration procedures at the volume edge.

After registration, layers containing retinal capillaries were extracted by manually identifying and removing the inner limiting membrane, outer nuclear layer, and all layers that fell outside these two. What remained were only those layers with retinal vasculature. An en face projection of this sub-volume was used to determine the horizontal and vertical diameters of the FAZ (i.e., as visually identified in the projection). This involved measuring (degrees) the distance between capillaries at opposite edges of the FAZ (nasal to temporal; inferior to superior). Next, 10 capillaries within 100 μm of the FAZ edge were randomly selected. No preference was given to capillary appearance other than that the capillary had to be visually distinguishable from the background reflectance. A-scan traces of their linear intensity profile were $4\times$ oversampled (zero padding in Fourier domain), registered, and averaged; from this a full-width-at-half-maximum (FWHM) width was determined. The FWHM measurement protocol followed that used by Hammer et al.[24] except that we measured the diameter of the capillary only in the axial direction. Note that we confined our measurements to those parts of the capillaries in which we could confirm the orientation as perpendicular to the incident UHR-AO-OCT beam, thereby avoiding the need to account for angle differences. We also chose to measure axial width as opposed to lateral width to avoid obvious errors that would have been incurred by the 9-μm sampling of B-scans. Last, we determined the depth range of retinal capillaries (shallowest to deepest) as a function of retinal eccentricity (0°–1.25°). Capillary depth was manually identified along eight radial lines (45° intervals) that subtended 360° and intersected at the deepest position in the fovea pit, as identified in the UHR-AO-OCT volume.

Procedure for Entoptic Experiment

The entoptic method was administered to the same seven volunteers and was used as an independent measure of the FAZ. Using a through-the-pupil Maxwellian-view entoptoscope (described in detail elsewhere[15]), subjects were asked to fixate on the central portion of a 15° field of uniform blue light (447 nm). Absorption of blue light by the retinal vasculature projects a high contrast shadow pattern onto the underlying photoreceptors. The subject was instructed to draw the vasculature pattern on paper, paying attention to the defining edges of the FAZ, if it was observed. Subjects were permitted to view their drawing and the entoptic shadow as long as they wanted and were given as much practice and time as desired. None of the subjects were provided information about their UHR-AO-OCT images. Next, the horizontal and vertical dimensions of the subject's FAZ were measured by the subject adjusting the size of the blue field (controlled by an adjustable, circular diaphragm in the entoptoscope (see Ref. 15 for details) until its horizontal and vertical extent matched that of their entoptic FAZ. The adjustment procedure was repeated three times for each direction (horizontal and vertical) and required approximately 5 minutes per subject.

RESULTS

UHR-AO-OCT volumes and entoptic drawings of the foveal region were successfully obtained on the seven subjects. Representative UHR-AO-OCT volumes (extracted capillary subregions) are shown for subjects 2 and 7 in Figure 1. In the UHR-AO-OCT volumes, retinal capillaries and other retinal vasculature appear bright on a dim background, reflecting more light than the surrounding neural tissue. The neural reflection is not altogether inconsequential, however, becoming appreciable with increased inner retina thickness, as evident in the
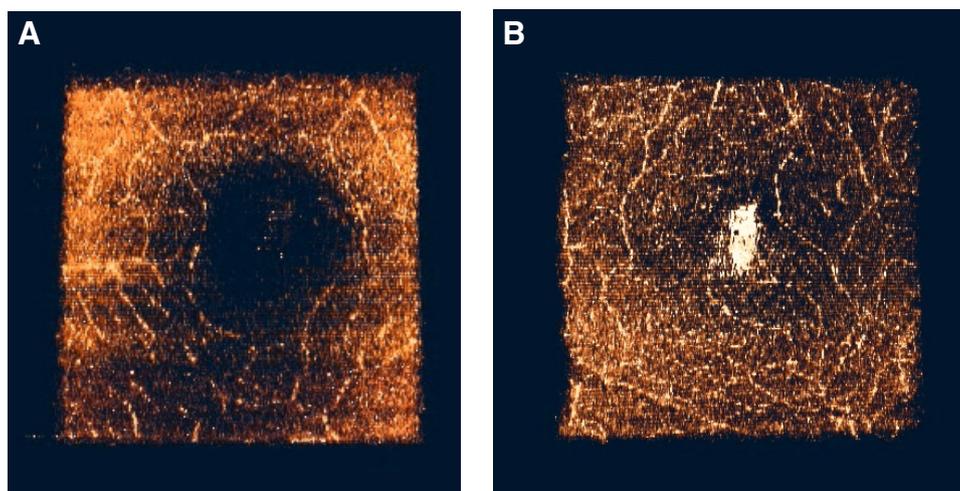

FIGURE 1. UHR-AO-OCT volumes (extracted capillary subregion) showing the foveal region in two subjects, one with a well-defined FAZ (**a**) and the other without (**b**). Dimensions of the volumes are 895 × 100 × 100 voxels (width × length × depth) that correspond to 891 × 900 × 180 μm. The volumes subtend slightly less than 3° × 3° because of image cropping (typically, 10 A-scans were removed). Optimal focus for vessel clarity was 0.35 D (**a**) and 0.25 D (**b**), realized with the AOptix DM. Central bright spot in (**b**) is a residual of the fovea reflex that was not completely removed in postprocessing when the capillary subregion was extracted. As evident, the UHR-AO-OCT volumes contained visible image artifacts. The high-magnification image—necessary for viewing microscopic details at the level of individual capillaries—exacerbates the effect of speckle noise (which is intrinsic to the interferometric nature of OCT) and the 9-μm gap between consecutive B-scans. Both noise and gap are comparable to the diameter of the capillaries. Speckle noise reduces the contrast of capillaries, and the gaps between B-scans disrupt the continuity of individual capillaries in the volume. Although both result in obvious image degradation, the volumes nevertheless retain the relevant information needed for the comparison study and for extracting quantitative information (FAZ size; capillary diameter; capillary depth range). The supplementary videos (Supplementary Movies S1 and S2) can be downloaded at http://www.iovs.org/lookup/suppl/doi:10.1167/iovs.10-6424/-/DCSupplemental.

FIGURE 2. UHR-AO-OCT images (**a, c**) and entoptic drawings (**b, d**) of the FAZ in two subjects: subject 3 (*top*) and subject 1 (*bottom*). Central bright spot in volumes is a residual of the fovea reflex that was not completely removed in postprocessing. (**b**) Subject 3 has a well-defined FAZ in addition to an adjacent rectangular region that is free of capillaries (distinct capillary feature) immediately nasal to the FAZ. (**a**) The UHR-AO-OCT volume is consistent with these entoptic observations, also suggesting a well-defined FAZ and a capillary free sub-region nasal to the FAZ. The drawing in (**d**) shows subject 1 also has a well-defined FAZ. The superior and inferior edges of the FAZ, however, are notably different from those of subject 3. The superior edge appears arch-like, and the inferior edge appears tortuous. (**c**) The UHR-AO-OCT volume image is consistent, showing a well-defined FAZ, a smooth superior capillary edge, and a tortuous inferior one.
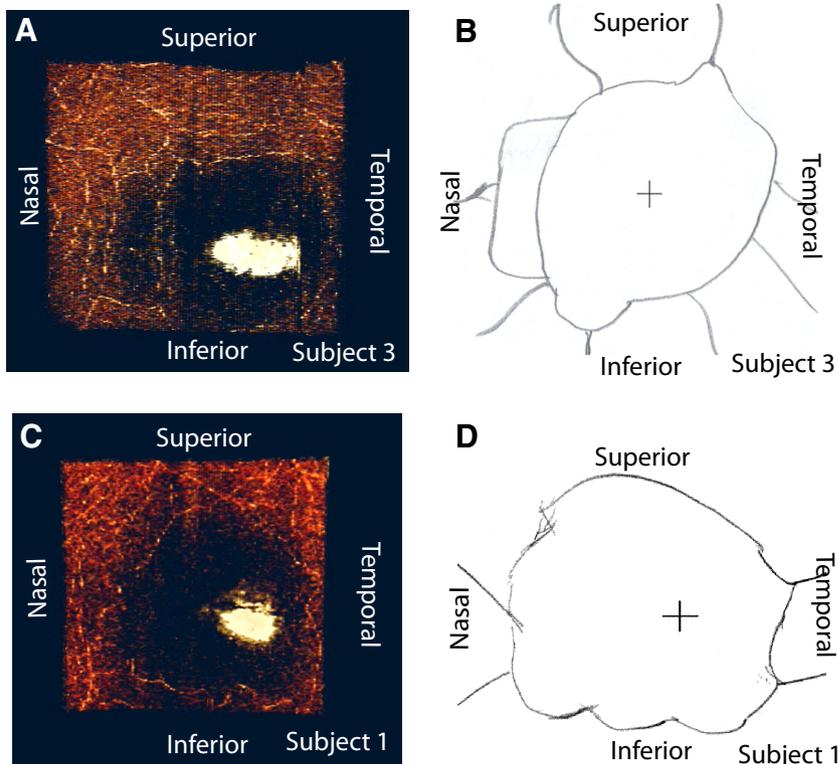
figure. The volume acquired on subject 2 (Fig. 1a) suggests a well-defined FAZ, composed of a capillary-free region (center of volume) surrounded by a network of capillaries. In comparison, the volume on subject 7 (Fig. 1b) suggests the absence of a FAZ with vessels traversing through the central fovea region where the zone would normally be.

FAZ Comparison of UHR-AO-OCT and Entoptic Methods

Next we compared the UHR-AO-OCT results with those obtained with the Maxwellian-view entoptoscope. Comparison involved testing for the presence of a FAZ, noting distinct features in the capillary pattern near the FAZ rim, and measuring the vertical and horizontal dimensions of the FAZ. Entoptic drawings were successfully obtained on the seven subjects; two representative drawings are shown in Figures 2b and 2d, along with the associated UHR-AO-OCT images (Figs. 2a, 2c). For these two subjects, the figure reveals strong similarities in the FAZ, as recorded by the two methods (details in figure legend). Similar observations were made on the other five subjects (not shown).

In 3 of the 7 subjects, the FAZ was missing, as determined with UHR-AO-OCT; this matched the entoptic observations. For the four subjects with a FAZ, Figure 3 shows the correlation between measured (UHR-AO-OCT) and predicted (entoptic viewing) FAZ diameters. The two are found strongly correlated ($R^2 = 0.862$).

Diameters of Capillaries near FAZ Edge

For each UHR-AO-OCT volume, 10 capillaries proximal to the FAZ edge were randomly selected, and their axial profiles were measured, registered, and averaged. As an example, Figure 4 shows the location of the 10 selected capillaries and the corresponding intensity profile (average and SD). The FWHM diameter for this subject is 4.6 μm. The average capillary diameter for each of the seven subjects is given in Figure 5.

Thickness of the Foveal Capillary Bed with Retinal Eccentricity

The depth range (shallowest to deepest) of capillaries observed in the UHR-AO-OCT volumes was measured as a function of retinal eccentricity (0°-1.25°). Results are plotted in Figure 6 and grouped by subjects with and without a FAZ. The figure shows that all subjects shared the same general trend: a monotonic increase in depth range with eccentricity. Differences
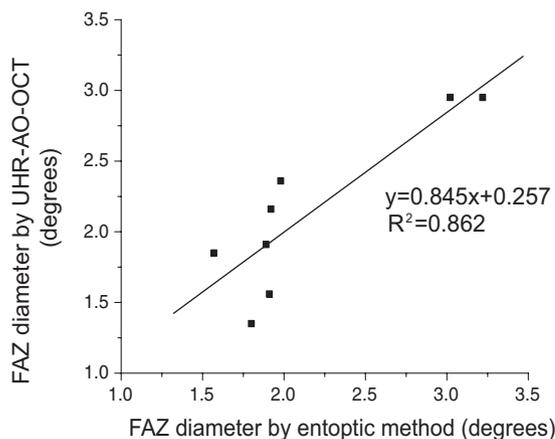

FIGURE 3. Correlation between UHR-AO-OCT and entoptic measurements of FAZ diameter. The plot contains horizontal and vertical measurements for the four subjects with a FAZ. *Solid line*: linear regression fit, which as a point of caution depends strongly on the two data points at approximately 3°. The FAZ for the entoptic measurements had an average diameter of 2.16° ± 0.60° and a range of 1.57° to 3.22°. For UHR-AO-OCT, the average was 2.09° ± 0.55° and the range 1.4° to 2.9°. The average absolute difference (percentage error) between the two methods was 9.3%. On average, UHR-AO-OCT undermeasured the FAZ size by 2.8% relative to entoptic viewing.
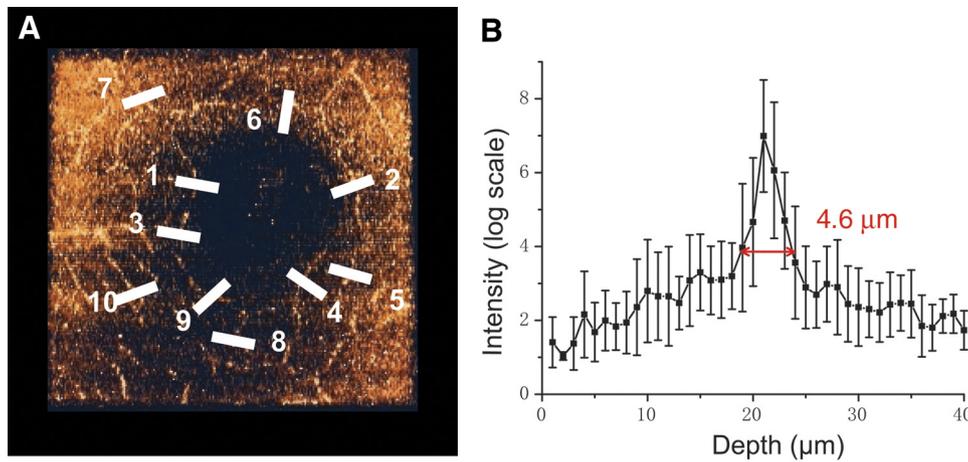
FIGURE 4. Average diameter of retinal capillaries near the FAZ as measured with UHR-AO-OCT in subject 2. (**a**) UHR-AO-OCT volume shows location of 10 capillary points (*white lines with numbers*) that were selected for diameter measurements. (**b**) The 10 measurements were registered, averaged, and plotted as shown. Error bars in the plot represent ±1 SD. FWHM diameter, defined at 3 dB below maximum,[30] is 4.6 μm.

between the two groups of subjects, however, are apparent. For subjects with a FAZ, a zero bed thickness (capillary-free region) extends from the fovea center out to approximately 1° (location denoted by dash arrows in the figure; see also FAZ dimensions in Fig. 3). At the maximum eccentricity measured (1.25°), the average depth range varied from 24 to 37 μm across the three subjects. For subjects without a FAZ, average depth range varied from 10 to 26 μm (foveal center) and 49 to 56 μm (1.25° eccentricity). The depth range of the subjects without a FAZ was consistently larger than that with, regardless of retinal eccentricity. In addition, subjects without exhibited considerably more variability in their own eyes, as indicated by the larger SD bars in Figure 6b than in Figure 6a. The average SD is 8.5 μm (without FAZ) compared with 1.2 μm (with FAZ) along different directions.

DISCUSSION

In this study, we investigated the capability of UHR-AO OCT to image individual capillaries in the fovea region, with emphasis on those that define the terminal rim of the FAZ. Use of the rim enabled comparison with entoptic viewing on the same eyes. Additional analysis of the UHR-AO-OCT volumes yielded mea-

FIGURE 5. Average diameters of retinal capillaries in subjects with (*left*) and without (*right*) a FAZ. Measurements were taken at the FAZ edge (*left*) and across the fovea (*right*). The average ± SD of capillary diameter is 5.4 ± 1.3 μm across the four subjects with a FAZ and 4.7 ± 1.7 μm across the three subjects without it. The average ± SD across all seven subjects is 5.1 ± 1.4 μm.

surements of capillary diameter and bed thickness with retinal eccentricity.

Validation of UHR-AO-OCT Using Entoptic Viewing

Validation of UHR-AO-OCT involved three parts: testing for the presence of a FAZ, noting distinct features in the capillary pattern near the FAZ rim, and measuring the size of the FAZ. To facilitate the first part, 3 of the 7 subjects were preselected with no FAZ. All volumes acquired with the UHR-AO-OCT showed clear evidence of the presence or absence of a FAZ, and this correctly matched the entoptic results. The two UHR-AO-OCT images in Figure 1 demonstrate how apparent it is to distinguish the two FAZ conditions. In short, UHR-AO-OCT was found just as effective as entoptic viewing at detecting microvasculature that protruded into the normally empty FAZ.

The second part took advantage of the fact that the FAZ vascular pattern varies significantly between eyes, making each pattern effectively unique. This was clearly evident in the four eyes that exhibited a FAZ. UHR-AO-OCT images for three of the eyes are shown in Figures 2 and 3. Note the obvious vascular differences among the three UHR-AO-OCT images; it would be difficult to mistake these as being from the same eye. Furthermore, distinct vascular features, such as the rectangular subregion free of capillaries of Figure 2a and the tortuous capillary pattern at the bottom of Figure 2c, are also suggestive in the entoptic drawings (Figs 2b, 2d). Although these observations are qualitative, the consistent finding of the same general capillary pattern across UHR-AO-OCT image and entoptic drawing provides further evidence that UHR-AO-OCT detects many of the capillaries proximal to the FAZ, many of which should be 4 to 5 μm in diameter.[33,34]

The third part was the most quantitative: correlating FAZ size measurements from UHR-AO-OCT and entoptic viewing. As shown in Figure 3, a strong correlation was found ($R^2 = 0.862$). Interestingly, one of the subjects had a noticeably larger (~3°) FAZ that was correctly detected with UHR-AO-OCT and barely fit into the instrument's field of view. Note that the regression slope and intercept ($y = 0.845x + 0.257$) deviates somewhat from the ideal $y = x$ line, indicating systematic errors in the data. These errors likely did not originate from noise in the UHR-AO-OCT data because the capillaries could be readily identified in the images, and variations in repeated measurements were negligible relative to the average absolute difference of 9.3% between the two methods. Furthermore, UHR-AO-OCT did not consistently overestimate or underestimate the FAZ size,
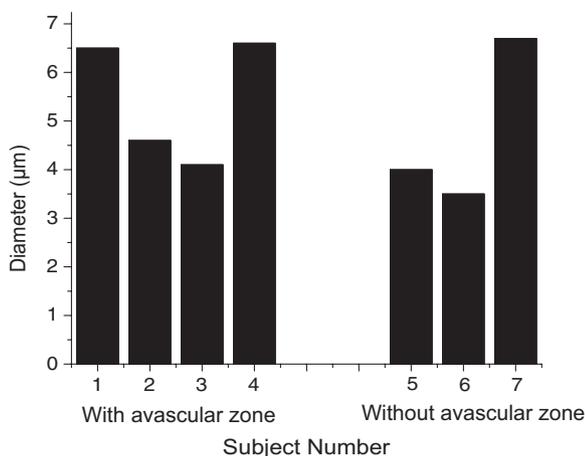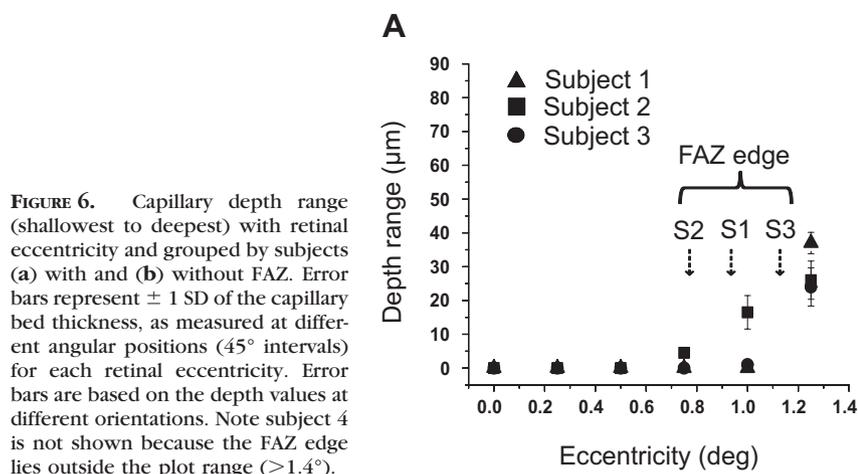
FIGURE 6. Capillary depth range (shallowest to deepest) with retinal eccentricity and grouped by subjects (**a**) with and (**b**) without FAZ. Error bars represent ± 1 SD of the capillary bed thickness, as measured at different angular positions (45° intervals) for each retinal eccentricity. Error bars are based on the depth values at different orientations. Note subject 4 is not shown because the FAZ edge lies outside the plot range (>1.4°).
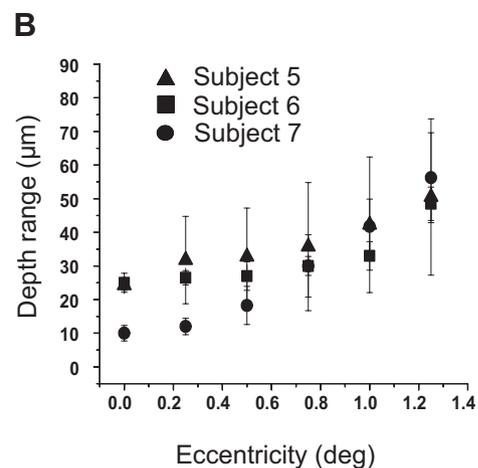
indicating a system calibration error. UHR-AO-OCT overestimated two subjects and underestimated the other two. A plausible explanation, which points to a potential weakness of our test, is the use of a circular diaphragm in the entoptoscope to measure the FAZ. Irregularities in the FAZ shape are commonplace and distort the shape from circular, in some cases noticeably (up to 20%). Thus, though the subjects demonstrated good precision (well below the 9.3% average absolute difference) in repeated adjustments of the circular diaphragm, obvious judgment by the subject was required to determine the best match between diaphragm and FAZ in the horizontal and vertical meridians. Consistent with this, the subject with the most distorted FAZ gave the worst agreement between the two methods. Given this uncertainty plus the striking differences in how these two methods work (psychophysics compared with optical imaging), an average absolute difference of 9.3% should not be surprising.

In summary, UHR-AO-OCT yielded results consistent with those on entoptic viewing. UHR-AO-OCT correctly detected the three subjects missing a FAZ, delineated unique features in the FAZ boundary that qualitatively matched those produced by entoptic viewing, and yielded FAZ dimensions (width and height) that were strongly correlated with entoptic viewing. All evidence points to the conclusion that UHR-AO-OCT can detect the small capillaries that define the rim of the FAZ.

Diameters of Capillaries near FAZ Rim

Next, UHR-AO-OCT was used to measure the axial profile of capillaries proximal to the FAZ. Average diameter across the seven subjects was 5.1 ± 1.4 μm, with a range of 3.5 μm to 6.7 μm. The range fits well within those reported by Weinhaus et al.[33] (2.5–7 μm) and Snodderly et al.[34] (2.5–10 μm). Weinhaus et al.[33] also reported average diameters of 4.7 ± 0.8 μm, 4.5 ± 0.7 μm, and 4.7 ± 0.8 μm for capillaries residing in the ganglion cell, shallow inner nuclear, and deep inner nuclear layers of the retina. These three layers are believed to contribute predominantly to the capillaries near the FAZ and thus were likely the capillaries we observed with UHR-AO-OCT. Indeed, the UHR-AO-OCT average value of 5.1 μm is consistent with the capillary sizes of these layers, the small but significant approximately 0.5-μm difference not withstanding.

A likely source for the 0.5-μm difference is blurring caused by the 3.3-μm coherence length (axial resolution), which is not accounted for in our diameter measurements. As a first-order estimate of what the actual diameter is, we

modeled the imaging process with Fourier optics and used Gaussian functions to represent the axial point spread function and capillary cross-section. Based on this model, the actual average diameter is estimated to be 4.6 μm (instead of 5.1μm), with an actual range of 2.6 μm to 6.3 μm instead of 3.5 μm to 6.7 μm. These estimates come strikingly close to the reported histology.

In short, the consistency of UHR-AO-OCT measurements of capillary size with histology provides substantive evidence that UHR-AO-OCT is capable of imaging a large portion of the capillaries proximal to the FAZ, certainly capillaries at least as small as 5 μm and likely smaller. Outside the fovea, retinal scatter (which increases with retinal depth) may degrade the image quality of deeper capillaries because it is well known to do so for fluorescein angiography. However, unlike fluorescein angiography, UHR-AO-OCT provides extremely fine optical sectioning (3 μm) and, if needed, can be combined with phase-sensitive detection to increase vasculature contrast.[41] Although capillary imaging at all depths in the retina with UHR-AO-OCT is likely possible, this remains to be tested.

Comparison of capillary diameters of the four subjects with and the three subjects without a FAZ revealed that the former had somewhat larger capillaries (5.6 μm vs. 4.7 μm), but the difference was not statistically significant (*t*-test value: −0.76). This finding does not support that of Hammer et al.[24] in which high-resolution (HR-)AO-OCT was used on 10 subjects to measure capillary diameters in retinopathy of prematurity (ROP without FAZ) and on those without it (control with FAZ). Average diameters of 11.6 μm (control with FAZ) and 7.5 μm (ROP without FAZ) were reported, and the difference was significant. Unfortunately, we could not investigate the potential influence of ROP on capillary size in our subjects because documented history of ROP was unavailable. This issue aside, however, any comparison would have been hampered by the large discrepancy in capillary size between the two studies. The average diameters reported by Hammer et al.[24] (11.6 μm and 7.5 μm) are noticeably larger than ours and those of the two histologic studies. In fact, the 11.6-μm diameter falls well outside the range of both histologic studies. Perhaps the added axial resolution of UHR-OCT (compared with HR-OCT) and attention to focus at the capillary plane are necessary for such measurements.

Depth Range of Capillaries with Retinal Eccentricity

It is well known that the retinal vasculature is laminated with capillary beds located at discrete depths in the retina.[42]

Near the fovea, beds occur in the nerve fiber layer and ganglion cell layer, and two straddle the inner nuclear layer. At the FAZ rim, only the inner nuclear layer beds exist and form effectively one layer because of the shrinking thickness of the retina in the fovea pit. Here we investigated the capability of UHR-AO-OCT, with its $3\text{-}\mu m$ axial resolution, to measure the collective depth range (shallowest to deepest) of these layers as a function of retinal eccentricity ($0°\text{-}1.25°$). Figure 6 shows depth changes on the order of tens of microns are readily detectable with UHR-AO-OCT. In Figure 6a, the capillary-free region extends to approximately $1°$ (indicated by dash arrows), the edge of which was confirmed to be of capillaries in the inner nuclear layer. The 30- to $40\text{-}\mu m$ thickness jump at roughly $1.25°$ reflects the onset of capillaries in the ganglion layer, which is consistent with the formation of capillary layers in the fovea as reported with histology.[33,34]

Regardless of retinal eccentricity, the average depth range of the capillaries was always greater in subjects without than in subjects with a FAZ (compare Figs 6a and 6b). This condition must obviously hold at eccentricities inside the FAZ area, but it also holds at larger eccentricities where both subject groups have an abundance of capillaries. The larger range is consistent with the findings of Hammer et al.,[24] who observed appreciably thicker inner retinal layers for ROP subjects.

CONCLUSION

Current reports of AO-OCT imaging of the retinal vasculature imply faithful imaging of the fine capillary networks. By comparing to entoptic viewing on the same eyes, we show that UHR-AO-OCT with careful focusing is indeed capable of imaging many of the capillaries proximal to the FAZ, including those of average size ($\sim 4.7\ \mu m$), as predicted by histology. This suggests that the vast majority of capillaries in the retina are likely detectable with UHR-AO-OCT, though increased instrument sensitivity may be required to offset increased scatter when the retina becomes thick and the capillaries are deep. This remains to be investigated. Aside from this caveat, UHR-AO-OCT is a promising option for noninvasive mapping of the intricate details of the multilaminar networks of capillaries in the retina. Future technological advances—for example, high-speed OCT imaging using recently reported line scan detectors[25,43] and phase detection[41]—will only improve on the results presented here.

References

1. Ballerini L. Genetic snakes for medical images segmentation. *Math Modeling Estimation Techn Comput Vision.* 1998;3457:284–295.
2. Ibanñez MV, Simó A. Bayesian detection of the fovea in eye fundus angiographies. *Pattern Recognition Lett.* 1999;20:229–240.
3. Conrath J, Valat O, Giorgi R, et al. Semi-automated detection of the foveal avascular zone in fluorescein angiograms in diabetes mellitus. *Clin Exp Ophthalmol.* 2006;34:119–123.
4. Zheng Y, Gandhi JS, Stangos AN, Campa C, Broadbent DM, Harding SP. Automated segmentation of foveal avascular zone in fundus fluorescein angiography. *Invest Ophthalmol Vis Sci.* 2010;51:3653–3659.
5. Wolf S, Arend O, Toonen H, Bertram B, Jung F, Reim M. Retinal capillary blood flow measurement with a scanning laser ophthalmoscope. *Ophthalmology.* 1991;98:996–1000.
6. Arend O, Wolf S, Jung F, et al. Retinal microcirculation in patients with diabetes mellitus: dynamic and morphological analysis of perifoveal capillary network. *Br J Ophthalmol.* 1991;75:514–518.
7. Arend O, Harris A, Shoemaker JA, et al. Perifoveal capillary microcirculation: comparison of blue light simulation and scanning laser technique. *Invest Ophthalmol Vis Sci.* 1993;34:1391.
8. Yap M, Gilchrist J, Weatherill J. Psychophysical measurement of the foveal avascular zone. *Ophthal Physiol Opt.* 1987;7:405–410.
9. Zeffren BS, Applegate RA, Bradley A, van Heuven WAJ. Retinal fixation point location in the foveal avascular zone. *Invest Ophthalmol Vis Sci.* 1990;31:2099–2105.
10. Bradley A, Applegate RA, Zeffren BS, van Heuven WAJ. Psychophysical measurement of the size and shape of the human foveal avascular zone. *Ophthal Physiol Opt.* 1992;12:18–23.
11. Bird AC, Weale RA. On the retinal vasculature of the human fovea. *Exp Eye Res.* 1974;19:409–417.
12. Riva CE, Petrig BL. Blue field entoptic phenomenon and blood velocity in the retinal capillaries. *J Opt Soc Am A.* 1980;70:1234–1238.
13. Petrig BL, Riva CE. Optimal strategy in using the blue field simulation technique for the measurement of macular blood flow. *Tech Digest Ser.* 1990;3:76–79.
14. Boer P, Hofstetter HW. An entoptic method for the measurement of eccentric fixation in amblyopia ex anopsia. *Am J Optom Arch Am Acad Optom.* 1972;49:417–422.
15. Bradley A, Zhang H, Applegate RA, Thibos LN, Elsner AE. Entoptic image quality of the retinal vasculature. *Vis Research.* 1998;38:2685–2696.
16. Martin JA, Roorda A. Direct and noninvasive assessment of parafoveal capillary leukocyte velocity. *Ophthalmology.* 2005;112:2219–2224.
17. Zhang Z, Petrig BL, Qi X, Burns SA. In vivo measurement of erythrocyte velocity and retinal blood flow using adaptive optics scanning laser ophthalmoscopy. *Opt Express.* 2008;16:12746–12756.
18. Tam J, Martin JA, Roorda A. Noninvasive visualization and analysis of parafoveal capillaries in humans. *Invest Ophthalmol Vis Sci.* 2010;51:1691–1698.
19. Rha J, Jonnal RS, Thorn KE, Qu J, Zhang Y, Miller DT. Adaptive optics flood-illumination camera for high speed retinal imaging. *Opt Express.* 2006;14:4552–4569.
20. Hermann B, Fernandez EJ, Unterhuber A, et al. Adaptive-optics ultrahigh-resolution optical coherence tomography. *Opt Lett.* 2004;29:2142–2144.
21. Zhang Y, Rha J, Jonnal RS, Miller DT. Adaptive optics parallel spectral domain optical coherence tomography for imaging the living retina. *Opt Express.* 2005;13:4792–4811.
22. Zhang Y, Cense B, Rha J, et al. High-speed volumetric imaging of cone photoreceptors with adaptive optics spectral-domain optical coherence tomography. *Opt Express.* 2006;14:4380–4394.
23. Zawadzki RJ, Jones SM, Olivier SS, et al. Adaptive-optics optical coherence, tomography for high-resolution and high-speed 3D retinal in vivo imaging. *Opt Express.* 2005;13:8532–8546.
24. Hammer DX, Iftimia NV, Ferguson RD, et al. Foveal fine structure in retinopathy of prematurity: an adaptive optics Fourier domain optical coherence tomography study. *Invest Ophthalmol Vis Sci.* 2008;49:2061–2070.
25. Torti C, Považay B, Hofer B, et al. Adaptive optics optical coherence tomography at 120,000 depth scans/s for non-invasive cellular phenotyping of the living human retina. *Opt Express.* 2009;17:19382–19400.
26. Kurokawa K, Sasaki K, Makita S, et al. Simultaneous high-resolution retinal imaging and high-penetration choroidal imaging by one-micrometer adaptive optics optical coherence tomography. *Opt Express.* 2010;18:8515–8527.
27. Zawadzki RJ, Cense B, Zhang Y, Choi SS, Miller DT, Werner JS. Ultrahigh-resolution optical coherence tomography with monochromatic and chromatic aberration correction. *Opt Express.* 2008;16:8126–8143.
28. Wojtkowski M, Bajraszewski T, Gorczyńska I, et al. Ophthalmic imaging by spectral optical coherence tomography. *Am J Ophthalmol.* 2004;138:412–419.
29. Fujimoto JG, Drexler W, Schuman JS, Hitzenberger CK. Optical coherence tomography (OCT) in ophthalmology: introduction. *Opt Express.* 2009;17:3978–3979.
30. Cense B, Koperda E, Brown JM, et al. Volumetric retinal imaging with ultrahigh-resolution spectral-domain optical coherence tomography and adaptive optics using two broadband light sources. *Opt Express.* 2009;17:4095–4111.

31. Zawadzki RJ, Choi SS, Jones SM, Olivier SS, Werner JS. Adaptive optics-optical coherence tomography: optimizing visualization of microscopic retinal structures in three dimensions. *J Opt Soc Am A.* 2007;24:1373–1383.

32. Zawadzki RJ, Choi SS, Fuller AR, Evans JW, Hamann B, Werner JS. Cellular resolution volumetric in vivo retinal imaging with adaptive optics-optical coherence tomography. *Opt Express.* 2009;17: 4084–4094.

33. Weinhausa RS, Burkea JM, Delori FC, Snodderly DM. Comparison of fluorescein angiography with microvascular anatomy of macaque retinas. *Exp Eye Res.* 1995;61:1–16.

34. Snodderly DM, Weinhaus RS, Choi JC. Neural-vascular relationships in central retina of Macaque monkeys (*Macaca fascicularis*). *J Neurosci.* 1992;12:1169-l193.

35. Springer AD, Hendrickson AE. Development of the primate area of high acuity, 1: use of finite-element analysis models to identify mechanical variables affecting pit formation. *Vis Neurosci.* 2004; 21:53–62.

36. Springer AD, Hendrickson AE. Development of the primate area of high acuity, 2: quantitative morphological changes associated with retina and pars plana growth. *Vis Neurosci.* 2004;21:775–790.

37. Springer AD, Hendrickson AE. Development of the primate area of high acuity, 3: temporal relationships between pit formation, retinal elongation and cone packing. *Vis Neurosci.* 2005;2:171–185.

38. Provis JM, Hendrickson AE. The foveal avascular region of developing human retina arch. *Ophthalmology.* 2008;126:507–511.

39. Mintz-Hittner HA, Knight-Nanan DM, Satriano DR, Kretzer FL. A small foveal avascular zone may be an historic mark of prematurity. *Ophthalmology.* 1999;106:1409–1413.

40. Delori FC, Webb RH, Sliney DH. Maximum permissible exposures for ocular safety (ANSI 2000), with emphasis on ophthalmic devices. *J Opt Soc Am A.* 2007;24:1250–1265.

41. Fingler J, Zawadzki RJ, Werner JS, Schwartz D, Fraser SE. Volumetric microvascular imaging of human retina using optical coherence tomography with a novel motion contrast technique. *Opt Express.* 2009;17:22190–22200.

42. Oyster CW. *The Human Eye: Structure and Function*. Sunderland, MA: Sinauer Associates, Inc.; 1999.

43. Potsaid B, Gorczynska I, Srinivasan VJ, et al. Ultrahigh speed spectral/Fourier domain OCT ophthalmic imaging at 70,000 to 312,500 axial scans per second. *Opt Express*. 2008;16:15149–15169.